Phase diagram of fluid phases in ^{3}He-^{4}He mixtures

N. Farahmand Bafi,[1,2,*] A. Maciołek,[1,2,3,†] and S. Dietrich[1,2,‡]

[1]*Max-Planck-Institut für Intelligente Systeme, Heisenbergstr. 3, D-70569 Stuttgart, Germany*

[2]*IV. Institut für Theoretische Physik, Universität Stuttgart, Pfaffenwaldring 57, D-70569 Stuttgart, Germany*

[3]*Institute of Physical Chemistry, Polish Academy of Sciences, Kasprzaka 44/52, PL-01-224 Warsaw, Poland*

(Received 25 November 2014; published 26 February 2015; corrected 23 July 2015)

Fluid parts of the phase diagram of ^{3}He-^{4}He mixtures are obtained from a mean-field analysis of a suitable lattice gas model for binary liquid mixtures. The proposed model takes into account the continuous rotational symmetry O(2) of the superfluid degrees of freedom associated with ^{4}He and includes the occurrence of vacancies. This latter degree of freedom allows the model to exhibit a vapor phase and hence can provide the theoretical framework to describe the experimental conditions for measurements of tricritical Casimir forces in ^{3}He-^{4}He wetting films.

DOI: 10.1103/PhysRevE.91.022138 PACS number(s): 05.50.+q, 64.60.De, 64.60.Kw, 67.60.−g

I. INTRODUCTION

Binary mixtures of the helium isotopes ^{3}He and ^{4}He exhibit a very rich phase behavior due to the presence of pronounced quantum effects. For example, below a certain threshold value of the pressure the zero-point fluctuations of the helium atoms demolish the solid phase. Accordingly, the liquid phase persists down to temperature $T = 0$. The solid phase forms only at high pressures, whereas for sufficiently low pressures and $T > 0$ helium forms the vapor phase. The bulk phase diagram of ^{4}He is shown schematically in Fig. 1. The liquid phase can be either a normal fluid or superfluid. These two fluid phases are separated by a line of second-order phase transitions, which is called the λ-line. This line terminates at the critical end points ce$^+$ and ce at the liquid-solid and liquid-vapor coexistence lines, respectively. The liquid-vapor coexistence line terminates at the critical point c.

Adding ^{3}He atoms to the pure ^{4}He liquid dilutes the ^{4}He carriers of superfluidity and thus lowers the critical temperature of the superfluid transition. (Superfluid transitions of ^{3}He atoms occur at very low temperatures, which are not considered here.) Beyond a certain dilution due to ^{3}He atoms the superfluid transition turns into a first-order phase transition; this occurs at a tricritical point tc. The schematic phase diagram of ^{3}He-^{4}He mixtures at fixed pressure is shown in Fig. 2. The transition temperature T_λ of the second-order phase transition to the superfluid phase depends on the concentration X_3 of ^{3}He atoms. For temperatures below the tricritical point tc, the mixture undergoes a first-order superfluid-normal phase transition which is accompanied by a two-phase region.

The schematic phase diagram of ^{3}He-^{4}He mixtures in the (T, Z, P) space, where Z is the fugacity of ^{3}He, is shown in Fig. 3 [1]. In the plane $Z = 0$, i.e., in the case of pure ^{4}He, the phase diagram is the same as the one in Fig. 1. A_1 and A_2 are the surfaces of first-order solid-liquid and vapor-liquid transitions, respectively, whereas A_3 and A_4 are the surfaces of second- and first-order phase transitions, respectively, between the superfluid and the normal fluid. Accordingly, A_3 and A_4 are separated by a line TC of tricritical points, which terminates at the tricritical end points tce$^+$ and tce. The points tce$^+$ and ce$^+$ as well as tce and ce are connected by lines of critical end points on A_1 and A_2, respectively. The surface A_4 intersects the surfaces A_1 and A_2 along triple lines of three-phase coexistence between the solid and the two liquid phases and the vapor and the two liquid phases, respectively.

Classical lattice models have turned out to successfully describe the essential features of the phase diagram of binary liquid mixtures. Such a model for describing the phase diagram of ^{3}He-^{4}He mixtures near the tricritical point was first introduced and studied by Blume, Emery, and Griffiths (called the BEG model) [2]. In this classical spin-1 model, the superfluid order parameter is mimicked by two discrete values; the remaining possible value for the state variable indicates whether a lattice site is occupied by a ^{3}He atom instead of a ^{4}He atom. Since this interpretation of the spin-1 model does not allow for vacancies, it does not exhibit a vapor phase. Furthermore, due to the discrete values assigned to the superfluid order parameter, this model does not capture the actual complex character of the superfluid order parameter. Another interpretation of the BEG model is to allow for vacant sites in a *classical* binary liquid mixture of species A and B, which leads to the formation of an A-rich liquid, a B-rich liquid, a mixed fluid phase, and a vapor phase. Such a model has been used to study the condensation and the phase separation in binary liquid mixtures [3–5]. The reduced phase diagrams of ternary mixtures have also been studied within this model [6].

Further improvements in the theoretical description of the phase diagrams of ^{3}He-^{4}He mixtures have been achieved by enriching the classical spin-1/2 model (i.e., without vacancies) by a continuous value for the superfluid order parameter. Although this model takes into account the continuous O(2) symmetry of the superfluid order parameter, it does not incorporate the occurrence of a vapor phase. Such a model with no vacancies and O(2) symmetry of the superfluid order parameter is given by the so-called vectorized BEG (VBEG) model, which has been proposed and studied in two dimensions ($d = 2$) by Cardy and Scalapino [7] and, independently, by Berker and Nelson [8]. More recently it has been investigated in $d = 3$ within mean-field theory and by Monte Carlo simulations [9].

In order to be able to study wetting films in ^{3}He-^{4}He mixtures which have been used to analyze experimentally the

*nimabafi@is.mpg.de
†maciolek@is.mpg.de
‡dietrich@is.mpg.de

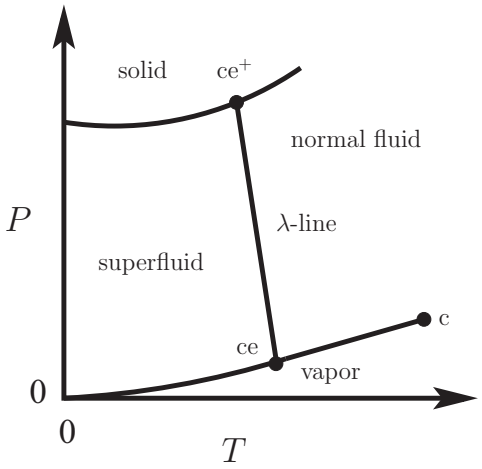

FIG. 1. Schematic bulk phase diagram of ^{4}He exhibiting the vapor, superfluid, normal fluid, and solid phases. The liquid-vapor critical point is denoted by c, whereas ce$^+$ and ce are critical end points. The λ-line is the line of second-order phase transitions between the superfluid and the normal fluid.

tricritical Casimir effect [10], the theoretical description of ^{3}He-^{4}He mixtures requires us to take into account the occurrence of a vapor phase. Tricritical Casimir forces acting on the liquid-vapor interface of ^{3}He-^{4}He wetting films arise due to the confinement of the tricritical fluctuations of the superfluid order parameter and of the composition near the tricritical point of the mixture. The considerable interest in this subject has been triggered both by theoretical predictions [1,11] and by experiments in which superfluid wetting films (^{4}He [12,13] and ^{3}He-^{4}He [10]) were used to provide reliable evidence for critical Casimir forces. Specifically, concerning tricriticality, a ^{3}He-^{4}He mixture was prepared in a thermodynamic state

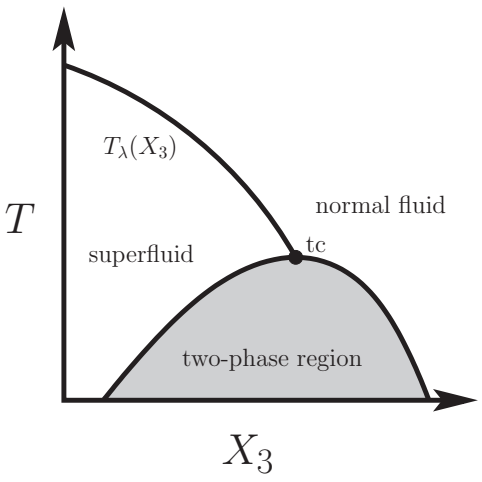

FIG. 2. Schematic bulk phase diagram of ^{3}He-^{4}He mixtures at fixed pressure. X_3 is the concentration of ^{3}He and $T_\lambda(X_3)$ is the line of continuous superfluid transitions, which turn into first-order superfluid transitions at the tricritical point tc. Note that $T_\lambda(X_3)$ meets the two-phase region at its top. If $T_\lambda(X_3)$ met the two-phase region below T_{tc}, this would imply that there is a discontinuous phase transition either between two normal fluid phases or between two superfluid phases, which is not the case.

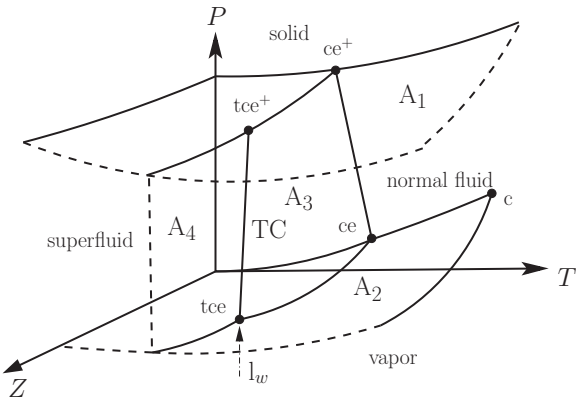

FIG. 3. Schematic phase diagram of ^{3}He-^{4}He mixtures in the (T, Z, P) space, where $Z = \exp(\mu_3/T)$ is the fugacity of ^{3}He and P is the pressure. A_1 and A_2 are the surfaces of the first-order solid-liquid and vapor-liquid phase transitions, respectively, whereas A_3 and A_4 are the surfaces of second- and first-order phase transitions between the normal fluid and the superfluid, respectively. A_3 intersects A_1 and A_2 along a line of critical end points connecting ce$^+$ with tce$^+$ and ce with tce, respectively. The surfaces A_3 and A_4 are separated by a line of tricritical points TC which meets A_1 and A_2 at the tricritical end points tce$^+$ and tce, respectively. A_2 terminates at a line of critical points, starting from c in the plane $Z = 0$. The phase diagram in the plane $Z = 0$ is the same as the one in Fig. 1. The dashed lines have no physical meaning; they indicate that the corresponding surface continues. The arrow l_w indicates the thermodynamic path along which tricritical end point wetting occurs.

of the vapor phase, close to coexistence with the liquid phase. Upon decreasing undersaturation (see the thermodynamic path l_w in Fig. 3), a complete wetting film was grown at the plates of capacitors, the equilibrium thickness of which could be determined very accurately from capacitance measurements. From the balance of the effective forces acting on the depinning liquid-vapor interface such as to thicken or to thin the film, the universal scaling function of the tricritical Casimir force was determined.

At present, the only available corresponding theoretical analysis [14] of the behavior of the tricritical Casimir scaling functions describing the ^{3}He-^{4}He wetting film thicknesses employs the VBEG model without vacancies and thus does not incorporate the vapor phase. Within this simplified approach, the wetting films have been modeled by a slab geometry with the boundaries introduced by fiat and not of via the actual self-consistent formation as a wetting film. Therefore, it is an open question how the critical Casimir forces emerge in the ^{3}He-^{4}He wetting films when the system is brought towards the critical or the tricritical end point, i.e., approaching liquid-vapor coexistence from the vapor side. The present bulk analysis is a prerequisite of such investigations.

The model proposed here is a classical spin-1 model, including the continuous O(2) symmetry of the superfluid order parameter, which does allow for vacant sites and therefore exhibits a vapor phase if the number of vacant sites is sufficiently large. The phase diagrams of this model are obtained within mean-field theory. Since there are three order parameters (i.e., the number densities of ^{3}He and ^{4}He as well as the order parameter corresponding to the superfluid transition),

the phase diagrams of the proposed model exhibit a rich diversity of topologies. The main difficulty of the present study resides in extracting from a high-dimensional parameter space the range of parameters for which the phase diagrams have the topology corresponding to the actual ^{3}He-^{4}He mixtures. In the next section we introduce the model and continue by obtaining various features of the phase diagram. We close with a summary and conclusions.

II. THE MODEL

We consider a three-dimensional ($d = 3$) simple cubic lattice with lattice spacing $a = 1$. The lattice sites $\{i \mid i = 1, \ldots, \mathcal{N}\}$ are occupied by either ^{3}He or ^{4}He or they are unoccupied. The Hamiltonian of this system is

$$\mathcal{H} = -J_{44}N_{44} - J_{33}N_{33} - J_{34}N_{34} - \mu_4 N_4 - \mu_3 N_3 - J_s\tilde{N}_{44} - \mathbf{H}\cdot\tilde{\mathbf{N}}_4, \quad (1)$$

where N_{mn}, with $m,n \in \{3,4\}$, denotes the number of pairs of nearest neighbors of species m and n on the lattice sites, N_m denotes the number of atoms of species m, and $-J_s\tilde{N}_{44}$ denotes the sum of the interaction energy between the superfluid degrees of freedom Θ_i and Θ_j associated with the nearest-neighbor pairs $\langle i,j\rangle$ of ^{4}He with J_s as the corresponding interaction strength. J_{33}, J_{44}, and J_{34} describe the effective interactions between the three types of pairs of He isotopes. The ^{3}He-^{3}He and ^{4}He-^{4}He pair potentials between the isotopes are not quite the same due to the slight differences in their electronic states. Moreover, the corresponding effective interactions differ due to the distinct statistics of the two isotopes. The chemical potential of species m is denoted as μ_m. $\mathbf{H} = (H_x, H_y)$ is the field conjugate to the superfluid degrees of freedom given by the vector $(\cos\Theta_i, \sin\Theta_i)$, provided that the lattice site i is occupied by a ^{4}He atom. (In ^{3}He-^{4}He mixtures treated as a mixture of ideal Bose and Fermi gases the phase transition to the superfluid phase depends only on the concentration of ^{4}He atoms. In the present model this is captured by the last two terms in Eq. (1). However, a refined theory such as the present one takes into account that the exchange interactions between the three possible pairs of helium isotopes affect the concentrations of the two species and thus implicitly influence the phase transition to the superfluid phase.)

In order to proceed, we express N_m and N_{mn} in terms of occupation numbers of the lattice sites $\{i\}$. We associate with each lattice site i an occupation variable s_i which can take the three values $+1$, -1, or 0, where $+1$ means that the lattice site is occupied by ^{4}He, -1 means the lattice site is occupied by ^{3}He, and 0 means the lattice site is unoccupied. Accordingly, one has

$$N_4 = \frac{1}{2}\sum_i s_i(s_i+1) \equiv \sum_i p_i,$$

$$N_3 = \frac{1}{2}\sum_i s_i(s_i-1),$$

$$N_{44} = \frac{1}{4}\sum_{\langle i,j\rangle}(s_i(s_i+1)s_j(s_j+1)) \equiv \sum_{\langle i,j\rangle} p_i p_j,$$

$$N_{33} = \frac{1}{4}\sum_{\langle i,j\rangle}(s_i(s_i-1)s_j(s_j-1)),$$

$$N_{34} = \frac{1}{4}\sum_{\langle i,j\rangle}[s_i(s_i+1)s_j(s_j-1) + s_i(s_i-1)s_j(s_j+1)], \quad (2)$$

where $\sum_{\langle i,j\rangle}$ denotes the sum over nearest neighbors. Using the above definitions one obtains

$$\mathcal{H} = -K\sum_{\langle i,j\rangle} s_i s_j - J\sum_{\langle i,j\rangle} q_i q_j - C\sum_{\langle i,j\rangle}(s_i q_j + q_i s_j) - \Delta_-\sum_i s_i - \Delta_+\sum_i q_i - J_s\sum_{\langle i,j\rangle} p_i p_j\cos(\Theta_i - \Theta_j) - H_x\sum_i p_i\cos\Theta_i - H_y\sum_i p_i\sin\Theta_i, \quad (3)$$

where

$$\sum_{\langle i,j\rangle} p_i p_j\cos(\Theta_i - \Theta_j) = \tilde{N}_{44} = \sum_{\langle i,j\rangle} p_i p_j \begin{pmatrix}\cos\Theta_i\\ \sin\Theta_i\end{pmatrix}\begin{pmatrix}\cos\Theta_j\\ \sin\Theta_j\end{pmatrix},$$

$$\sum_i p_i(\cos\Theta_i, \sin\Theta_i) = \tilde{\mathbf{N}}_4, \quad (4)$$

and

$$\begin{aligned} q_i &= s_i^2,\\ p_i &= \tfrac{1}{2}s_i(s_i+1),\\ K &= \tfrac{1}{4}(J_{44} + J_{33} - 2J_{34}),\\ J &= \tfrac{1}{4}(J_{44} + J_{33} + 2J_{34}),\\ C &= \tfrac{1}{4}(J_{44} - J_{33}),\\ \Delta_- &= \tfrac{1}{2}(\mu_4 - \mu_3),\\ \Delta_+ &= \tfrac{1}{2}(\mu_4 + \mu_3), \end{aligned} \quad (5)$$

and $\Theta_i \in [0, 2\pi]$ represents the superfluid degree of freedom at the lattice site i, provided it is occupied by ^{4}He.

III. MEAN-FIELD THEORY

In this section we apply mean-field theory to the above model. This approximation follows from a variational method based upon approximating the total equilibrium density matrix by a product of density matrices associated with each lattice site [15].

Due to the variation principle, the free energy F obeys the following inequality:

$$F \leqslant \phi = \hat{\mathrm{Tr}}(\rho\mathcal{H}) + (1/\beta)\hat{\mathrm{Tr}}(\rho\ln\rho), \quad (6)$$

where ρ is any trial density matrix with $\hat{\mathrm{Tr}}(\rho) = 1$, with respect to which ϕ on the right-hand side of Eq. (6) should be minimized in order to obtain the best approximation;

$$\hat{\mathrm{Tr}} = \sum_{s_1=\pm1,0}\int_0^{2\pi} d\Theta_1 \cdots \sum_{s_{\mathcal{N}}=\pm1,0}\int_0^{2\pi} d\Theta_{\mathcal{N}} \quad (7)$$

denotes the trace and $\beta = 1/T$, where T is the temperature times k_B. The mean-field approximation assumes that any lattice site experiences the same mean field generated by its neighborhood so the total density matrix will be the product of the density matrices corresponding to each lattice site:

$$\rho = \prod_i \rho_i, \tag{8}$$

with

$$\mathrm{Tr}\rho_i = \sum_{s_i=\pm1,0} \int_0^{2\pi} d\Theta_i \rho_i(s_i,\Theta_i) = 1. \tag{9}$$

For homogeneous bulk systems the local density matrix is independent of the site.

The variational mean-field free energy per site for the Hamiltonian introduced in the previous section is [with $\cos(\Theta_i - \Theta_j) = \cos\Theta_i \cos\Theta_j + \sin\Theta_i \sin\Theta_j$]

$$\begin{aligned}\frac{\phi}{\mathcal{N}} = &-\frac{z}{2}[K\langle s_i\rangle^2 + J\langle q_i\rangle^2 + 2C\langle q_i\rangle\langle s_i\rangle \\ &+ J_s(\langle p_i\cos\Theta_i\rangle^2 + \langle p_i\sin\Theta_i\rangle^2)] \\ &- \Delta_-\langle s_i\rangle - \Delta_+\langle q_i\rangle - H_x\langle p_i\cos\Theta_i\rangle - H_y\langle p_i\sin\Theta_i\rangle \\ &+ (1/\beta)\mathrm{Tr}(\rho_i\ln\rho_i),\end{aligned} \tag{10}$$

where $\mathcal{N}$ is the total number of sites and z is the coordination number of the lattice ($z = 2d$, where d is the spatial dimension of the system; here $z = 6$) and $\langle\dots\rangle = \mathrm{Tr}(\rho_i\dots)$ denotes the thermal average, taken with the trial density matrix ρ_i associated with the lattice site i.

Minimizing the variational function $\phi/\mathcal{N}$ with respect to ρ_i renders the best normalized functional form of ρ_i. There are two approaches to find the variational minima. In the first approach one parametrizes the density matrix ρ_i in terms of the order parameters of the phase transitions and minimizes $\phi/\mathcal{N}$ with respect to the coefficients multiplying these order parameters. In the second approach one treats ρ itself as a variational function and minimizes $\phi/\mathcal{N}$ with respect to it [15]. We follow the second approach and calculate the functional derivative of $\phi/\mathcal{N}$ in Eq. (10) with respect to $\rho_i(s_i,\Theta_i)$ using $\frac{\delta\rho_i(s_i,\Theta_i)}{\delta\rho_j(s_j,\Theta_j)} = \delta(\Theta_i - \Theta_j)\delta_{s_i,s_j}$ and equate it to the Lagrange multiplier η corresponding to the constraint $\mathrm{Tr}(\rho_i) = 1$,

$$\begin{aligned}\eta = &\frac{\delta(\phi/\mathcal{N})}{\delta\rho_i(s_i,\Theta_i)} \\ = &-z[K\langle s_i\rangle s_i + J\langle q_i\rangle q_i + C(q_i\langle s_i\rangle + \langle q_i\rangle s_i) \\ &+ J_s(\langle p_i\cos\Theta_i\rangle p_i\cos\Theta_i + \langle p_i\sin\Theta_i\rangle p_i\sin\Theta_i)] \\ &- \Delta_- s_i - \Delta_+ q_i - H_x p_i\cos\Theta_i - H_y p_i\sin\Theta_i \\ &+ (1 + \ln\rho_i)/\beta.\end{aligned} \tag{11}$$

Equation (11) can be solved for $\rho_i(s_i,\Theta_i)$:

$$\rho_i = e^{\beta\eta - 1 - \beta h_i}, \tag{12}$$

where

$$\begin{aligned}h_i(s_i,\Theta_i) = &- s_i(kX + cD + \Delta_-) - q_i(jD + cX + \Delta_+) \\ &- p_i[(j_s M_x + H_x)\cos\Theta_i + (j_s M_y + H_y)\sin\Theta_i]\end{aligned} \tag{13}$$

is the single-site Hamiltonian in which the coupling constants are rescaled as $j = zJ$, $c = zC$, $k = zK$, $j_s = zJ_s$ and where the following order parameters are introduced:

$$\begin{aligned}X &:= \langle s_i\rangle, \\ D &:= \langle q_i\rangle, \\ M_x &:= \langle p_i\cos\Theta_i\rangle, \\ M_y &:= \langle p_i\sin\Theta_i\rangle,\end{aligned} \tag{14}$$

which in the bulk are independent of i. In accordance with Eq. (4) one has $\langle\tilde{\mathbf{N}}_4\rangle = \mathcal{N}\mathbf{M}$. The normalization $\mathrm{Tr}(\rho_i) = 1$ yields

$$e^{-\beta\eta+1} = \mathrm{Tr}(e^{-\beta h_i}) \tag{15}$$

so

$$\rho_i = \frac{e^{-\beta h_i}}{\mathrm{Tr}(e^{-\beta h_i})}, \tag{16}$$

where h_i is given by Eq. (13).

The order parameters defined in Eq. (14) allow one to determine the number densities $X_4 = \frac{\langle N_4\rangle}{\mathcal{N}} = \frac{D+X}{2}$ and $X_3 = \frac{\langle N_3\rangle}{\mathcal{N}} = \frac{D-X}{2}$ so $X = (\langle N_4\rangle - \langle N_3\rangle)/\mathcal{N} = X_4 - X_3$ is the difference of the number densities and $D = (\langle N_4\rangle + \langle N_3\rangle)/\mathcal{N}$ is the total number density. The concentration of ^{4}He and ^{3}He is $\frac{\langle N_4\rangle}{\langle N_4\rangle+\langle N_3\rangle} \equiv \mathcal{C}_4 = \frac{D+X}{2D} = X_4/D$ and $\frac{\langle N_3\rangle}{\langle N_4\rangle+\langle N_3\rangle} \equiv \mathcal{C}_3 = \frac{D-X}{2D} = X_3/D$, respectively. M_x and M_y are the components of the two-dimensional superfluid order parameter $\mathbf{M} = (M_x, M_y)$ with $M := \sqrt{|\mathbf{M}|^2} = \sqrt{M_x^2 + M_y^2}$. The equilibrium superfluid order parameter $\mathbf{M}$ points into the direction of $\mathbf{H}$. This follows from the principle of minimum free energy together with the relation $\frac{\partial F}{\partial \mathbf{H}} = -\mathbf{M}$, where F is the free energy of the system, which implies that for fixed T, Δ_+, and Δ_- one has $dF = -d\mathbf{H}\cdot\mathbf{M}$. Thus for $\mathbf{H}$ with an orientation ψ, i.e., $\mathbf{H} = (H_x, H_y) = H(\cos\psi, \sin\psi)$ with $H := \sqrt{|\mathbf{H}|^2} = \sqrt{H_x^2 + H_y^2}$, $\mathbf{M}$ points into the same direction, i.e., $\mathbf{M} = (M_x, M_y) = M(\cos\psi, \sin\psi)$.

Within the aforementioned mean-field approximation the order parameters $X(\Delta_-,\Delta_+,H,T) = \mathrm{Tr}(\rho_i s_i)$, $D(\Delta_-,\Delta_+,H,T) = \mathrm{Tr}(\rho_i q_i)$ and $M(\Delta_-,\Delta_+,H,T)$ [with the latter obtained from $M_x = \mathrm{Tr}(\rho_i p_i\cos\Theta_i)$ and $M_y = \mathrm{Tr}(\rho_i p_i\sin\Theta_i)$] are given by three coupled self-consistent equations:

$$X = \frac{-W(X,D;\Delta_-,\Delta_+,H,T) + R(X,D;\Delta_-,\Delta_+,H,T)I_0(\beta j_s M + \beta H)}{1 + W(X,D;\Delta_-,\Delta_+,H,T) + R(X,D;\Delta_-,\Delta_+,H,T)I_0(\beta j_s M + \beta H)}, \tag{17}$$

$$D = \frac{W(X,D;\Delta_-,\Delta_+,H,T) + R(X,D;\Delta_-,\Delta_+,H,T)I_0(\beta j_s M + \beta H)}{1 + W(X,D;\Delta_-,\Delta_+,H,T) + R(X,D;\Delta_-,\Delta_+,H,T)I_0(\beta j_s M + \beta H)}, \tag{18}$$

and

$$M = \frac{R(X,D;\Delta_-,\Delta_+,H,T)I_1(\beta j_s M + \beta H)}{1 + W(X,D;\Delta_-,\Delta_+,H,T) + R(X,D;\Delta_-,\Delta_+,H,T)I_0(\beta j_s M + \beta H)}, \tag{19}$$

where I_0 and I_1 are modified Bessel functions (see Sec. 9.6 in Ref. [16]). The functions $W(X,D;\Delta_-,\Delta_+,H,T)$ and $R(X,D;\Delta_-,\Delta_+,H,T)$ are given by

$$W(X,D;\Delta_-,\Delta_+,H,T) = e^{\beta[(c-k)X+(j-c)D+\Delta_+-\Delta_-]} > 0 \tag{20}$$

and

$$R(X,D;\Delta_-,\Delta_+,H,T) = e^{\beta[(c+k)X+(j+c)D+\Delta_++\Delta_-]} > 0 \tag{21}$$

so $D > X$. The equilibrium free energy $\phi(\Delta_-,\Delta_+,H,T)$ is given by

$$\phi(\Delta_-,\Delta_+,H,T) = \mathcal{N}\left[\frac{k}{2}X^2 + \frac{j}{2}D^2 + cXD + \frac{j_s}{2}M^2 + \frac{1}{\beta}\ln(1-D)\right]. \tag{22}$$

In the limit $\Delta_+ \to +\infty$ both W and R diverge so, according to Eq. (18), one has $D(\Delta_-,\Delta_+ \to +\infty,H,T) \to 1$, i.e., all lattice sites are occupied and the concentrations reduce to $\mathcal{C}_4 = (1+X)/2$ and $\mathcal{C}_3 = (1-X)/2$. With the explicit expressions in Eqs. (20) and (21), in the limit $\Delta_+ \to +\infty$, Eqs. (17) and (19) reduce to:

$$X = \frac{-e^{-\beta(2kX+2c+2\Delta_-)} + I_0(\beta j_s M + \beta H)}{e^{-\beta(2kX+2c+2\Delta_-)} + I_0(\beta j_s M + \beta H)}, \quad \Delta_+ = \infty, \tag{23}$$

and

$$M = \frac{I_1(\beta j_s M + \beta H)}{e^{-\beta(2kX+2c+2\Delta_-)} + I_0(\beta j_s M + \beta H)}, \quad \Delta_+ = \infty. \tag{24}$$

Expressing X in Eqs. (23) and (24) in terms of $\mathcal{C}_4$ renders

$$\mathcal{C}_4 = \frac{I_0(\beta j_s M + \beta H)}{e^{\beta(-\tilde{k}\mathcal{C}_4+\tilde{\Delta}_-)} + I_0(\beta j_s M + \beta H)}, \quad \Delta_+ = \infty, \tag{25}$$

and

$$M = \frac{I_1(\beta j_s M + \beta H)}{e^{\beta(-\tilde{k}\mathcal{C}_4+\tilde{\Delta}_-)} + I_0(\beta j_s M + \beta H)}, \quad \Delta_+ = \infty, \tag{26}$$

where $\tilde{k} = 4k$ and $\tilde{\Delta}_- = 2(-\Delta_- + k - c)$. For $H = 0$ these equations have the same form as the corresponding ones in Ref. [9], which do not allow for vacant sites from outset. Thus in the limit $\Delta_+ \to +\infty$ and for $H = 0$ our present more general results reduce to those of the more restricted model studied before.

IV. PHASE DIAGRAM

In this section we determine the phase diagram of the VBEG model within mean-field theory. Although certain features of the phase diagram can be obtained analytically, most parts of it can be determined only numerically. In order to find the coexisting states of phase equilibria, one has to identify those distinct states (X_ν, D_ν, M_ν), which share the same values for the chemical potentials and the pressure at a common temperature. The chemical potentials can be obtained by solving Eqs. (17) and (18) together with Eqs. (20) and (21) for Δ_+ and Δ_-:

$$\Delta_+(X,D,M;H,T) = \frac{T}{2}\ln(D^2-X^2) - T\ln(2(1-D)) - cX - jD - \frac{T}{2}\ln(I_0(j_sM/T + H/T)) \tag{27}$$

and

$$\Delta_-(X,D,M;H,T) = \frac{T}{2}\ln\frac{D+X}{D-X} - kX - cD - \frac{T}{2}\ln(I_0(j_sM/T + H/T)). \tag{28}$$

Within the grand-canonical ensemble the pressure is given by $\phi/\mathcal{N} = -P$. (Note that the sample volume is $V = \mathcal{N}a^3$, here with $a = 1$). According to Eqs. (17)–(19), the order parameters of any state must fulfill the relation

$$\frac{2M}{X+D} = \frac{M}{X_4} = \frac{I_1(\beta j_s M + \beta H)}{I_0(\beta j_s M + \beta H)}, \tag{29}$$

which expresses M in terms of $\frac{X+D}{2} = X_4$, T, and H. Depending on the value of the coupling constant j_s the phase diagram exhibits various topologies.

A. Phase diagram for a simple, normal liquid mixture: $j_s = 0$

For $j_s = 0$ and $H = 0$ there is no superfluid phase and M is always zero [compare Eq. (29) with $I_1(y \to 0) = \frac{1}{2}y$ and $I_0(y \to 0) = 1$]. For $j_s = 0$, due to $I_0(0) = 1$, the last term in Eq. (27) and in Eq. (28) drops out. Thus the phase diagram will be that of a simple binary normal liquid mixture of species 3 and 4, similar to the ones shown in Refs. [3–5]. The first-order demixing transitions occur at low temperatures, whereas at high temperatures the liquid is mixed. The demixing transitions terminate in a line of critical points which, due to $\frac{\partial\phi}{\partial X} = -\Delta_-$ [see Eqs. (10) and (14)], are given by [15]

$$\left.\frac{d\Delta_-}{dX}\right|_{\Delta_+,T} = \left.\frac{d^2\Delta_-}{dX^2}\right|_{\Delta_+,T} = 0, \quad \left.\frac{d^3\Delta_-}{dX^3}\right|_{\Delta_+,T} > 0, \tag{30}$$

where $\frac{d^n\Delta_-}{dX^n}|_{\Delta_+,T}$ denotes the n^{th} total derivative of Δ_- [see Eq. (28)] with respect to X at constant Δ_+ and T. Note that the independent variables are (T,Δ_+,Δ_-). Since Δ_- as given by Eq. (28) depends on D, which for $\Delta_+ = \text{const}$ in turn depends implicitly on X via Eq. (27), calculating the total derivative of Δ_- with respect to X requires the knowledge of the partial derivative of D with respect to X. Thus the first condition in Eq. (30) reads

$$\left.\frac{d\Delta_-}{dX}\right|_{\Delta_+,T} = \left.\frac{\partial\Delta_-}{\partial X}\right|_{\Delta_+,T} + \left.\frac{\partial\Delta_-}{\partial D}\frac{\partial D}{\partial X}\right|_{\Delta_+,T} = 0, \tag{31}$$

where $\frac{\partial\Delta_-}{\partial X}$ and $\frac{\partial\Delta_-}{\partial D}$ follow from Eq. (28) and where $\frac{\partial D}{\partial X}|_{\Delta_+,T}$ is obtained by taking the derivative of Eq. (27) with respect to X at fixed Δ_+ and T and by solving for $\frac{\partial D}{\partial X}|_{\Delta_+,T}$. Accordingly, the first condition in Eq. (30) leads to a quadratic equation:

$$T^2 + a_1 T + a_0 = 0, \tag{32}$$

with

$$a_1 = -D(-2cX + j + k) + X(kX - 2c) + D^2 j,$$
$$a_0 = (D-1)(D^2 - X^2)(c^2 - jk). \tag{33}$$

Equation (32) renders as a solution two branches $T_{1,2}(X,D)$. Similarly, the second condition in Eq. (30) leads to an equation $G(X,D,T) = 0$, where, due to the first condition, $T = T_{1,2}(X,D)$. Thus it takes the form $G(X,D,T_{1,2}(X,D)) =: g_{1,2}(X,D) = 0$. Therefore, for a given value $D^{(0)}$ of D, the solution of $g_{1,2}(X,D^{(0)}) = 0$ (which must be solved numerically) renders $X(D^{(0)}_{1,2}) = X^{(0)}_{1,2}$ so at $T^{(0)}_{1,2} = T_{1,2}(X^{(0)}_{1,2}, D^{(0)}_{1,2})$ the model exhibits a critical point, provided the condition $\frac{d^3\Delta_-}{dX^3}|_{\Delta_+,T} > 0$ is fulfilled. This latter condition and the physical constraints $T > 0$, $P > 0$, and $D > |X|$ exclude one of the two branches of $T_{1,2}(X,D)$. Thus, for various values of D, one obtains a set of points $\{(D, X(D), T(X(D),D))\}$, which forms a line of critical points in the space spanned by (X,D,T). According to Eqs. (27) and (28), the set $\{(D,X,T)\}$ can be transformed to the set $\{(\Delta_+(D,X;T), \Delta_-(D,X;T), T)\}$, which yields a line of critical points in the space spanned by (Δ_+, Δ_-, T). This line ends at the liquid-vapor coexistence surface forming a critical end point (see Fig. 4).

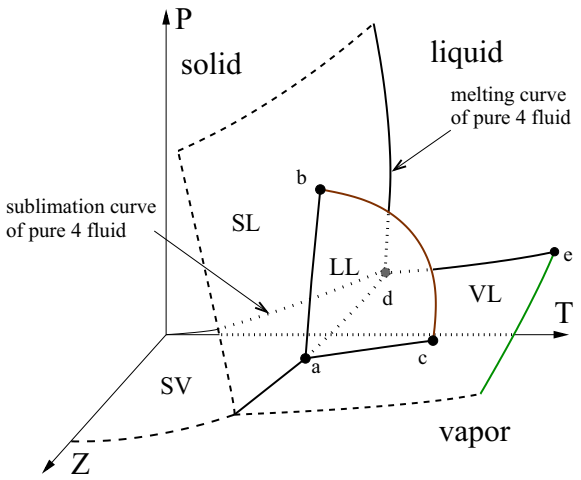

FIG. 4. (Color online) The schematic phase diagram for $H = 0$ and $j_s = 0$ (i.e., without coupling between the superfluid degrees of freedom). The phase diagram in the plane $Z = 0$ is that of a one-component system consisting of particles "4." Upon increasing the fugacity Z of particles "3," the transition lines in the plane $Z = 0$ extend to form three distinct surfaces. The surface SL is a surface of first-order phase transitions between the solid and the liquid phases. The transition surfaces between the vapor and the liquid phases, and between the solid and the liquid phases, are denoted by VL and SV, respectively. The surface VL terminates at a line of critical points (green line). The critical point of the pure system of "4" particles is denoted by e. The liquid can be either mixed or demixed. Concerning the demixed phases, LL denotes the surface of first-order phase transitions between the phase rich in component 3 (large Z) and the phase rich in the component 4 (small Z). This surface terminates at a line of critical points (brown line), which meets the surfaces SL and VL at the critical end points b and c, respectively. The point a is a quadruple point, whereas d is a triple point. The lines a-b, a-c, and a-d are triple lines. The dashed lines have no physical meaning; they indicate that the corresponding surfaces continue.

The schematic phase diagram for $j_s = 0$ in the (T,Z,P) space is shown in Fig. 4, with $Z = \exp(\mu_3/T)$. There are four surfaces separating various phases: the surface SL of first-order phase transitions between the solid and the liquid phases, the surface VL of first-order phase transitions between the vapor and the liquid phases, the surface SV of first-order

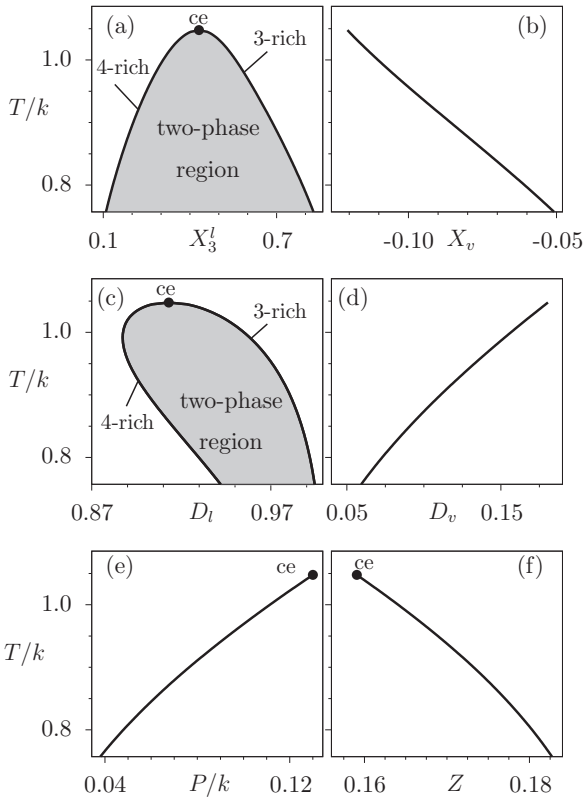

FIG. 5. Phase diagrams for the coupling constants $(c/k, j/k, j_s/k) = (1, 5.714, 0)$ and $H = 0$. Along the triple line of three-phase coexistence (see line a-c in Fig. 4) the figures show the first-order demixing transitions of the liquid at coexistence with the vapor phase (a) in the (X_3^l, T) plane, with $X_3^l = \langle N_3\rangle_l/\mathcal{N}$ corresponding to the 3-particles in the liquid phase; (b) in the (X_v, T) plane at coexistence with the two liquid phases, where $X_v = (\langle N_4\rangle_v - \langle N_3\rangle_v)/\mathcal{N}$ in the vapor phase; (c) in the (D_l, T) plane, where $D_l = (\langle N_4\rangle_l + \langle N_3\rangle_l)/\mathcal{N}$ in the liquid phase; and (d) in the (D_v, T) plane, where $D_v = (\langle N_4\rangle_v + \langle N_3\rangle_v)/\mathcal{N}$ in the vapor phase. The indices l and v refer to the values of the order parameters in the liquid and in the vapor phase, respectively. The critical end point ce here corresponds to the point c in Fig. 4. Panels (e) and (f) show the dependencies of the pressure P and of the fugacity $Z = \exp(\mu_3/T)$ on the temperature along the triple line a-c in Fig. 4. The two liquid states become identical at the critical end point ce at $T_{ce}/k = 1.947$, above which the liquid is mixed. The coexisting liquid and vapor phases at ce are $(X_l^{ce}, D_l^{ce}, M_l^{ce}) = (0.050, 0.913, 0)$ and $(X_v^{ce}, D_v^{ce}, M_v^{ce}) = (-0.120, 0.180, 0)$, respectively. The transitions between the vapor phase and the liquid phases are always first order. According to (e) and (f), along a-c both P and Z vary as function of T, with the requirement of staying in coexistence with the vapor phase. This implies that the white domains in (a) and (c) are not projections of a three-dimensional surface, given by the equation of state, onto the (T, X_3) and (T, D) plane, respectively. The black lines provide only the T dependence of X_3 and D_l along the line a-c, which contains two branches. Similar remarks hold for Figs. 9–12.

phase transitions between the solid and the liquid phases, and the surface LL of first-order phase transitions between the phase rich in component 3 and the phase rich in the component 4. This latter surface terminates at a line of critical points (brown line), and VL terminates at a line of critical points (green line).

In Fig. 5, the demixing transitions at coexistence with the vapor phase (see the line connecting the points a and c in Fig. 4) are shown for the coupling constants chosen as $(c/k, j/k, j_s/k) = (1, 5.714, 0)$. Along this triple line of first-order liquid-liquid transitions at coexistence with the vapor phase, three thermodynamic states with distinct number densities and concentrations coexist. The values of the order parameters of these three states are shown in Figs. 5(a)–5(d). The corresponding values of the pressure P/k and of the fugacity, $Z = \exp(\mu_3/T) = \exp(\frac{\mu_3}{k}\frac{1}{T/k})$ of the component 3 of the mixture ($\mu_3 = \Delta_+ - \Delta_-$ and T are rescaled by the coupling constant k), are shown in Figs. 5(e) and 5(f), respectively. The vapor phase is characterized by a small value D_v of the order parameter D, whereas a large value D_l of the density order parameter D corresponds to the liquid state. In Fig. 5, at fixed temperatures below the critical end point (ce) (which is denoted as c in Fig. 4), three values for X_3, i.e., two values X_3^l for X_3 in the liquid phases [Fig. 5(a)] and one value for the vapor phase [X_v in Fig. 5(b)], and three values for D [Figs. 5(c) and 5(d)] characterize the three states which share the same values of the pressure [Fig. 5(e)] and of the chemical potentials [and thus the fugacity, Fig. 5(f)]. At $T_{ce}/k = 1.947$ the two liquid states merge into a single state with $(X_l^{ce}, D_l^{ce}, M_l^{ce}) = (0.050, 0.913, 0)$, which coexists with the vapor state characterized by $(X_v^{ce}, D_v^{ce}, M_v^{ce}) = (-0.120, 0.180, 0)$. For $T > T_{ce}$ the liquid is mixed. The transitions between the vapor and the liquid phases are always first order, above and below T_{ce}.

B. Phase diagram including the superfluid phase: $j_s > 0$

For $j_s > 0$ the model exhibits superfluid transitions, which can be either first or second order. In order to find the surface of second-order phase transitions to the superfluid phase (see A_3 in Fig. 3), we introduce the appropriate thermodynamic potential A as the Legendre transform of ϕ:

$$A(\Delta_-, \Delta_+, M, T) = \phi(\Delta_-, \Delta_+, H(\Delta_-, \Delta_+, M, T), T) - M H(\Delta_-, \Delta_+, M, T), \tag{34}$$

where, according to Eq. (1), $\frac{\partial \phi(\Delta_-, \Delta_+, M, T)}{\partial H} = M$, which implicitly renders $H = H(\Delta_-, \Delta_+, M, T)$ so $\frac{\partial A(\Delta_-, \Delta_+, M, T)}{\partial M} = -H(\Delta_-, \Delta_+, M, T)$. In order to determine $H(\Delta_-, \Delta_+, M, T)$ we use Eq. (29). Because we are interested in the phase diagram for $H = 0$, we replace the right-hand side of Eq. (29) by its approximation linear in H:

$$\frac{2M}{X + D} = \frac{I_1(j_s M/T)}{I_0(j_s M/T)} + \frac{H}{T}\frac{I_1'(j_s M/T) I_0(j_s M/T) - I_0'(j_s M/T) I_1(j_s M/T)}{I_0^2(j_s M/T)}. \tag{35}$$

Solving this equation for H [using $I_0' = I_1$, $I_1' = (I_0 + I_2)/2$, and $I_2(a) = I_0(a) - \frac{2}{a} I_1(a)$] leads to

$$\begin{aligned} H &= \frac{I_1(j_s M/T)}{M/T}\frac{2M I_0(j_s M/T) - (X + D) I_1(j_s M/T)}{I_0^2(j_s M/T) + I_0(j_s M/T) I_2(j_s M/T) - 2 I_1^2(j_s M/T)} \\ &= \frac{-j_s T I_1(j_s M/T)[-2M I_0(j_s M/T) + (D + X) I_1(j_s M/T)]}{2[-j_s M (I_1(j_s M/T))^2 + I_0(j_s M/T)[T I_1(j_s M/T) + j_s M I_2(j_s M/T)]]}. \end{aligned} \tag{36}$$

Due to $\frac{\partial A}{\partial M} = -H$ the conditions for the critical points, where M vanishes continuously (see A_3 in Fig. 3), are [compare Eq. (30)]

$$\left.\frac{dH}{dM}\right|_{\Delta_+, \Delta_-, T} = \left.\frac{d^2 H}{dM^2}\right|_{\Delta_+, \Delta_-, T} = 0, \quad \left.\frac{d^3 H}{dM^3}\right|_{\Delta_+, \Delta_-, T} > 0, \tag{37}$$

with all total derivatives to be taken at $M = 0$ and at constant Δ_+, Δ_-, and T [compare Eq. (31)]. Note that the independent variables are (T, Δ_+, Δ_-). According to Eq. (36), calculating the total derivatives of H with respect to M requires the expression for $\frac{\partial H}{\partial M}$ and the knowledge of the partial derivatives of X and D with respect to M. These latter ones are obtained by taking the partial derivatives of Eqs. (27) and (28) with respect to M at fixed Δ_+ and Δ_- and by solving the resulting two coupled equations for the required derivatives $\frac{\partial X}{\partial M}$ and $\frac{\partial D}{\partial M}$.

Applying the conditions for critical points [Eq. (37)] leads to the following expression for the surface A_3 of superfluid transitions:

$$T_s = \frac{j_s}{4}(D + X). \tag{38}$$

We note that the same relation follows independently from Eq. (29) for $H = 0$ in the limit $M \to 0$. The route via Eq. (36) has, however, the additional advantage of facilitating also the calculation of tricritical points [see Eqs. (39)–(41)]. Furthermore, expanding the right-hand side of Eq. (29) up to and including the order H^3 leaves the result in Eq. (38) unchanged.

With D and X given by Eqs. (17)–(19) in terms of Δ_+, Δ_-, and T (note that $H = 0$ and that on this surface $M = 0$), Eq. (38) renders $T_s(\Delta_-, \Delta_+)$ which corresponds to a surface in the space spanned by (Δ_+, Δ_-, T).

This surface of second-order phase transitions between the normal fluid ($M = 0$) and the superfluid ($M \neq 0$) ends at the surface of liquid-vapor coexistence, forming a line of critical end points (see the line connecting ce and tce in Fig. 3). The

conditions for tricritical points are

$$\left.\frac{dH}{dM}\right|_{\Delta_+,\Delta_-,T} = \left.\frac{d^2H}{dM^2}\right|_{\Delta_+,\Delta_-,T} = \left.\frac{d^3H}{dM^3}\right|_{\Delta_+,\Delta_-,T} = \left.\frac{d^4H}{dM^4}\right|_{\Delta_+,\Delta_-,T} = 0, \quad \left.\frac{d^5H}{dM^5}\right|_{\Delta_+,\Delta_-,T} > 0, \tag{39}$$

with all total derivatives to be taken also at $M = 0$, which again requires us to consider the partial derivatives of X and D with respect to M, as discussed after Eq. (37). The vanishing of the first four derivatives leads to a quadratic equation for D [where Eq. (38) has been used to eliminate the dependence on T]:

$$b_2 D^2 + b_1 D + b_0 = 0, \tag{40}$$

where the coefficients $b_{0,1,2}$ are given in terms of the order parameter X and the coupling constants:

$$\begin{aligned} b_0 &= X[16c^2 - (4j + j_s)(4k + j_s)] \\ &\quad + X^2 j_s(4k + j_s), \\ b_1 &= 2X\left[j_s^2 - 8c^2 + 8jk + 2j_s(j + k)\right] \\ &\quad - (4c + j_s)^2 + 16jk, \\ b_2 &= 16c^2 + j_s(8c - 4k + j_s) - 16jk. \end{aligned} \tag{41}$$

We note that, also here, expanding the right-hand side of Eq. (29) up to and including the order H^2 does not change the results in Eqs. (40) and (41).

Accordingly, the solution of Eq. (40) yields $D = D_0(X)$ which, due to Eqs. (17)–(19), leads to the relation $D(\Delta_-,\Delta_+,T) = D_0(X(\Delta_-,\Delta_+,T))$. This turns into the relationship $T(\Delta_-,\Delta_+)$ which corresponds to a surface in the space spanned by (Δ_+,Δ_-,T). Simultaneously, Eq. (38) has to hold, which also corresponds to a surface in this space. Thus the tricritical points correspond to the intersection of these two surfaces and thus form a line of tricritical points (TC in Fig. 3). The condition for the fifth derivative along this line can be checked only numerically. This condition and the fact that $D > |X|$ exclude one of the two solutions of Eq. (40). For small values of j_s the model exhibits a superfluid transition in the liquid phase (see Fig. 6). In certain parts of the phase diagram this transition is second order, in other parts it is first order. Thus upon switching on j_s a new surface LL_3 raises above the bottom (i.e., VL) of the phase diagram shown in Fig. 4 and changes the character of the lower part of the surface LL in Fig. 4, indicated as LL_1, in Fig. 6.

The surface LL_3 of continuous transitions separates the superfluid and the normal fluid both 4-rich. The surface LL_1 corresponds to first-order phase transitions between the 4-rich superfluid and the 3-rich normal fluid. The surface $LL_1 \cup LL_2$ terminates LL_3 at a line f-i of critical end points.

Upon increasing the coupling constant j_s (Fig. 7), the model exhibits as a new feature a line j-k of tricritical points. In comparison with the phase diagram for weak j_s (Fig. 6), a new surface LL_4 emerges (j-k-f-i-j) which is the surface of first-order phase transitions between the superfluid and the normal fluid, both 4-rich (Fig. 7). The surface LL_3 of the second-order phase transitions between the superfluid and the normal fluid both 4-rich meet the surface LL_4 at a line of tricritical points (dark blue line j-k). LL_1 and LL_2 meet LL_4 at a triple line (i-f), where the superfluid and the 4-rich normal fluid coexist with the 3-rich normal fluid. Thus the increase of j_s changes the character of that part of LL_3 in Fig. 6, which is close to LL_2, from second-order to first-order phase transitions.

If the coupling constant j_s is increased further (Fig. 8), first-order phase transitions between liquid phases occur only between the superfluid and the normal fluid phase. There are no longer first-order demixing transitions between two normal fluids. Thus, upon increasing j_s, the surface $LL_3 \cup LL_4$ moves

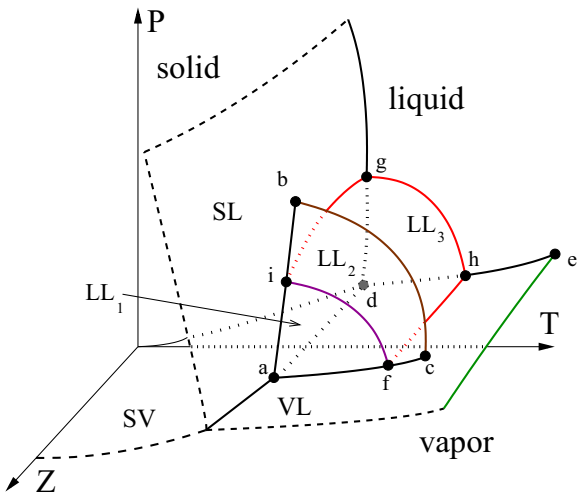

FIG. 6. (Color online) Schematic phase diagram for small values of j_s. SL, VL, and SV are surfaces of first-order phase transitions with the same meanings as in Fig. 4. The points denoted as g and h are critical end points of the continuous superfluid transition of the 4-pure fluid (i. e., $Z = 0$); g-h is the line of critical points for the continuous superfluid transition of the 4-pure fluid. LL_3 is a surface of continuous superfluid transitions bounded by the red lines g-h, h-f, i-g, and the violet line f-i. The triple point of the solid, vapor, and superfluid phases of the 4-pure fluid is denoted as d. In the plane $Z = 0$ the line to the left of d is the sublimation curve of the 4-pure fluid; d-h-e is the liquid-vapor coexistence line of the 4-pure fluid, which ends at its critical point e; the extension of the latter to $Z > 0$ forms the green line. The line d-g is the melting curve of the 4-pure solid into the superfluid and above g into the normal fluid. The line d-a is the triple line along which solid, vapor, and superfluid coexist; beyond a this line extends into a triple line along which solid, vapor, and normal fluid coexist. At the quadruple point a solid, vapor, normal fluid, and superfluid coexist. The surface $LL_1 \cup LL_2$, which corresponds to the surface LL in Fig. 4, is the surface of first-order transitions between the 4-rich liquid at the back and the 3-rich liquid in the front; it is bounded by the brown line b-c of critical points which connects the critical end points b and c. The surface $LL_1 \cup LL_2$ of first-order liquid-liquid demixing transitions terminates the surface LL_3 of continuous superfluid transitions. At this intersection this gives rise to the violet line f-i of critical end points, which themselves end at the end points i and f of this line of critical end points. At the surface LL_2 there are first-order phase transitions between two normal fluids, whereas at the surface LL_1 there are first-order phase transitions between a normal fluid with high concentration of 3-particles and a superfluid with high concentration of 4-particles. Accordingly, the superfluid phase forms a dome formed by the plane $Z = 0$, SL, VL, LL_3, and LL_1 with the vertices d, a, f, h, g, and i.

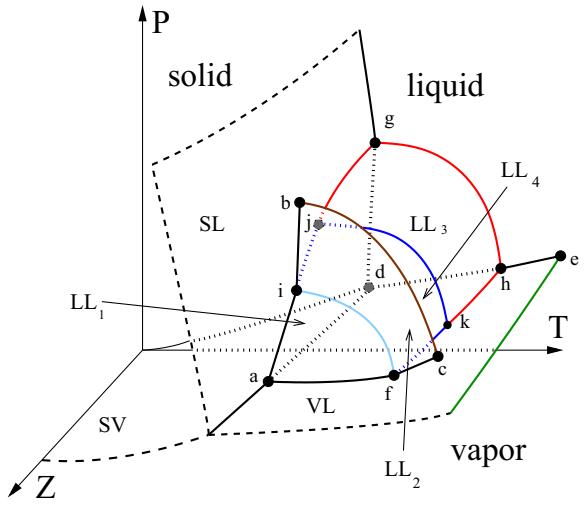

FIG. 7. (Color online) Schematic phase diagram for a value of j_s, for which both critical (b-c and LL_3) and tricritical (j-k) phase transitions between liquids occur. SL, VL, and SV are the surfaces of first-order phase transitions similar to those in Fig. 4. The superfluid dome is characterized the vertices a, f, k, h, g, d, j, and i. Outside this region the liquid is a normal fluid. LL_1 is the surface of first-order phase transitions between the 3-rich normal fluid and the 4-rich superfluid, LL_2 (enclosed by the lines i-b, b-c, c-f, and f-i) is the surface of first-order demixing phase transitions between 3-rich and 4-rich normal fluids, whereas LL_3 is the surface of second-order phase transitions between the normal fluid and the superfluid. The blue line (j-k) is the line of tricritical points where the surface LL_3 connects to the new surface LL_4 of first-order phase transitions between the normal fluid and the superfluid liquid phases both being 4-rich. The surfaces LL_2 and $LL_3 \cup LL_4$ meet at the line of triple points (light blue line i-f). The brown and the green lines are lines of critical points; a, i, and f are quadruple points, d is a triple point, whereas b, c, g, and h are critical end points. The line of triple points (i-f) ends on the surfaces SL and VL at the points i and f, respectively. The points j and k are tricritical end points. Note that in Fig. 6 the line i-f is a line of critical end points, whereas here it is a triple line. This different character motivates their different color code (violet versus light blue). This different character also implies that the lines a-i-b and a-f-c have a break in slope at i and f, respectively, here, but not in Fig. 6.

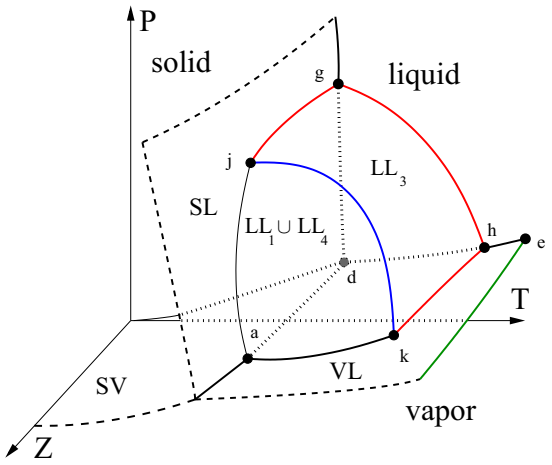

FIG. 8. (Color online) Schematic phase diagram for a value of j_s, for which only a tricritical line occurs. In this case, first-order phase transitions between liquid phases occur only between the superfluid and the normal fluid so the model exhibits only a (blue) line of tricritical points (j-k). SL, VL, and SV are the surfaces of first-order phase transitions as described in Fig. 4. The superfluid dome is characterized by the vertices a, k, h, g, d, and j. Outside this region the liquid is a normal fluid. The surface LL_2 from Fig. 7 does not exist anymore and the transitions between liquid phases are either second-order phase transitions between the normal fluid and the superfluid mixed liquid (LL_3) or first-order phase transitions between the normal fluid and the superfluid liquid ($LL_1 \cup LL_4$). The surfaces LL_3 and $LL_1 \cup LL_4$ meet at the line j-k of tricritical points (blue line). The points g and h are critical end points, whereas j and k are tricritical end points. The point a is a quadruple point and d is a triple point.

up (i.e., towards higher P and T) so, accordingly, the line i-f also moves up towards the line b-c. This implies that LL_2 shrinks and the wedge between the lines i-b and i-j becomes shorter. Finally, LL_2 and b-c disappear and LL_1 and LL_4 become a single surface of first-order transitions between 4-rich superfluid and 3-rich normal liquid; this implies that the line i-f disappears, too. Accordingly, the phase diagram is left with only a (blue) line of tricritical points k-j. This topology of the phase diagram is shown in Fig. 8. In this case the liquid-liquid phase transitions are either second-order phase transitions on LL_3 between the normal fluid and the superfluid mixed liquid or first-order phase transitions on $LL_4 \cup LL_1$ between the normal fluid and the superfluid liquid.

As discussed in the introduction, in the case of actual ^{3}He-^{4}He mixtures the solid phase is formed only at high pressures, whereas for sufficiently low pressures the superfluid reaches down to $T = 0$. In order to obtain this topology from that of Fig. 8, by fiat one has to pull up and tilt the surface SL and to shift the superfluid dome down to $T = 0$ so the surface SV disappears. This transforms the phase diagram in Fig. 8 to the one shown in Fig. 3 such that g = ce$^+$, h = ce, e = c, LL_3 = A_3, j-k = TC, j = tce$^+$, k = tce, and $LL_1 \cup LL_4$ = A_4. In this sense the bulk phase diagram shown in Fig. 8 is supposed to mimic the one of the actual ^{3}He-^{4}He mixtures.

The demixing transitions at coexistence with the vapor phase for various sets of the coupling constants are shown in Figs. 9–12. In these figures the values of c/k and j/k are the same; only the value of j_s is changed. For the choice of coupling constants $(c/k, j/k, j_s/k) = (1, 5.714, 1.717)$ (see Fig. 9), the phase diagram exhibits the topology of the schematic phase diagram shown in Fig. 6. The red line in Fig. 9(a) provides the temperature dependence of X_3 along the red line in Fig. 6 emanating from f towards h. The green point e in Fig. 9 corresponds to the point f in Fig. 6 and the black point in Fig. 9 corresponds to the point c in Fig. 6. Because in Fig. 6 the red line h-f is a line of continuous phase transitions right up to the point f, the line a-f-c does not exhibit a break in slope at f. Below e, the liquid transitions are first-order transitions between the normal fluid and the superfluid liquid, whereas above e the demixing curve remains the same as in the case of $j_s = 0$ (see Fig. 4).

As discussed in Fig. 7, for even larger values of j_s, both continuous and first-order superfluid transitions occur, giving rise to the occurrence of a line of tricritical points. For the choice of coupling constants $(c/k, j/k, j_s/k) = (1, 5.714, 2.231)$ and

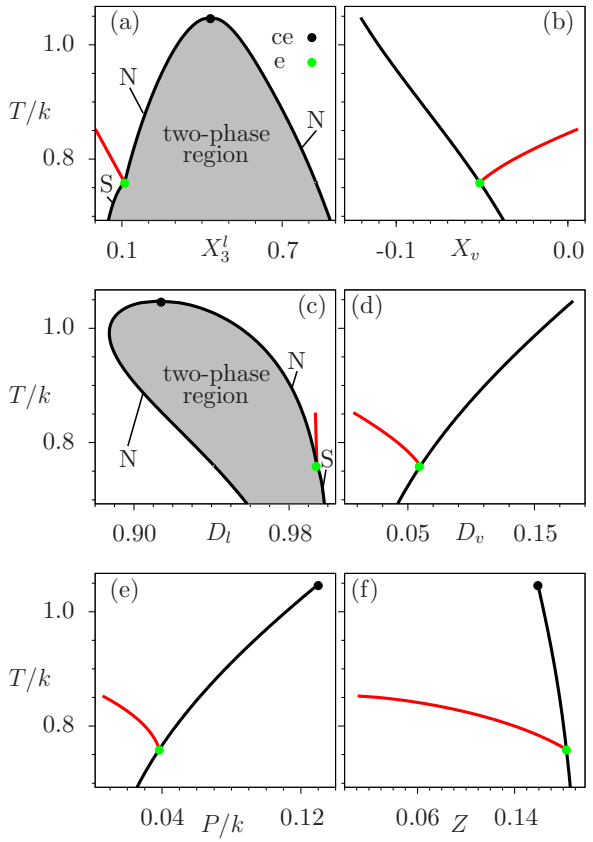

FIG. 9. (Color online) Phase diagram for the coupling constants $(c/k, j/k, j_s/k) = (1, 5.714, 1.717)$ and $H = 0$ corresponding to Fig. 6. Along the triple line a-f in Fig. 6 the figures show the coexistence between vapor, normal fluid, and superfluid (a) in the (X_3^l, T) plane, with $X_3^l = \langle N_3\rangle/\mathcal{N}$ corresponding to the number density of 3-particles in the liquid phase; (b) in the (X_v, T) plane at coexistence with the two liquid phases, where $X_v = (\langle N_4\rangle_v - \langle N_3\rangle_v)/\mathcal{N} = \langle X_4^v\rangle - \langle X_3^v\rangle$ in the vapor phase; (c) in the (D_l, T) plane, where $D_l = (\langle N_4\rangle_l + \langle N_3\rangle_l)/\mathcal{N}$ is the total number density in the liquid phase; and (d) in the (D_v, T) plane, where $D_v = (\langle N_4\rangle_v + \langle N_3\rangle_v)/\mathcal{N}$ is the total number density in the vapor phase. The indices l and v refer to the values of the order parameters in the liquid and the vapor phases, respectively. Panels (e) and (f) show the temperature dependence of P and Z along the triple line a-c Fig. 6 (black) and along the red line f-h near f in Fig. 6. The red line is the line of second-order transitions between the normal fluid and superfluid at coexistence with vapor, which ends at the demixing curve at the green critical end point e (i. e., f in Fig. 6). At e the liquid state $(X_l^e, D_l^e, M_l^e) = (0.773, 0.994, 0)$ coexists with the vapor state $(X_v^e, D_v^e, M_v^e) = (-0.051, 0.059, 0)$ at $T_e/k = 0.758$. N and S denote normal fluid and superfluid, respectively. The transitions between the vapor and the liquid phases are always first order. The points ce and e here correspond to the points c and f in Fig. 6.

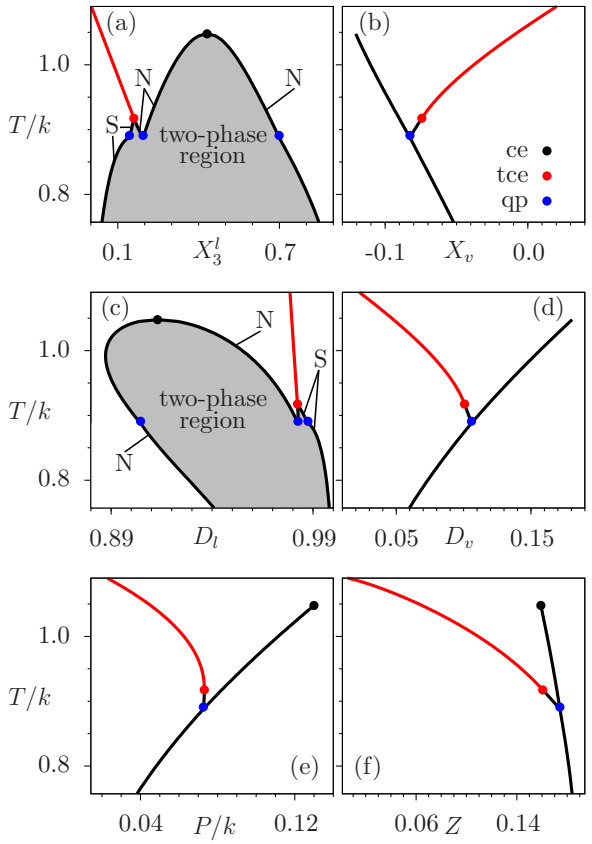

FIG. 10. (Color online) Phase diagram for the coupling constants $(c/k, j/k, j_s/k) = (1, 5.714, 2.231)$ and $H = 0$ which corresponds to Fig. 7. Along the triple lines a-f and f-c in Fig. 7 the figures show the first-order demixing transitions of the liquid phase at coexistence with the vapor phase (a) in the (X_3^l, T) plane, with $X_3^l = \langle N_3\rangle_l/\mathcal{N}$ as the number density of 3-particles in the liquid phase; (b) in the (X_v, T) plane at coexistence of the vapor with the two liquid phases, where $X_v = (\langle N_4\rangle_v - \langle N_3\rangle_v)/\mathcal{N}$ in the vapor phase; (c) in the (D_l, T) plane, where $D_l = (\langle N_4\rangle_l + \langle N_3\rangle_l)/\mathcal{N}$ in the liquid phase; and (d) in the (D_v, T) plane, where $D_v = (\langle N_4\rangle_v + \langle N_3\rangle_v)/\mathcal{N}$ in the vapor phase. The indices l and v refer to the values of the order parameters in the liquid and the vapor phases, respectively. Panels (e) and (f) show the temperature dependence of P and Z along the triple lines a-f, f-c, and f-k in Fig. 7. The red line corresponds to second-order phase transitions between normal fluids and superfluids (line k-h in Fig. 7). At tce, the liquid state $(X_l^{\rm tce}, D_l^{\rm tce}, M_l^{\rm tce}) = (0.662, 0.982, 0)$ coexists with the vapor state $(X_v^{\rm tce}, D_v^{\rm tce}, M_v^{\rm tce}) = (-0.074, 0.100, 0)$ at $T_{\rm tce}/k = 0.917$. The point ce remains as in the case $j_s = 0$. N and S denote normal liquid and superfluid, respectively. At the quadruple point qp the four coexisting states at $T_{\rm qp}/k = 0.887$ are two normal liquids $(X_l^{\rm qp}, D_l^{\rm qp}, M_l^{\rm qp}) = \{(-0.493, 0.904, 0), (0.594, 0.982, 0)\}$, a superfluid $(X_l^{\rm qp}, D_l^{\rm qp}, M_l^{\rm qp}) = (0.701, 0.987, 0.281)$, and the vapor state $(X_v^{\rm qp}, D_v^{\rm qp}, M_v^{\rm qp}) = (-0.082, 0.105, 0)$. The points ce, tce, and qp here correspond to the points c, k, and f, respectively in Fig. 7. In (b), (d)–(f), the long black coexistence curves are expected to exhibit a break in slope at qp; on the present scales this is not visible.

$(c/k, j/k, j_s/k) = (1, 5.714, 2.747)$ Figs. 10 and 11, respectively, show the liquid-liquid transitions at coexistence with the vapor phase for such a topology of the phase diagram. In both figures one finds two types of first-order liquid-liquid transitions, one between two normal liquids, which occur between ce and qp, and another one between the normal liquid phase and the superfluid liquid phase, which occur below tce. The points ce, tce, and qp in Figs. 10 and 11 correspond to the points c, k, and f, respectively, in Fig. 7. The transitions between the two normal liquids correspond to the line f-c in Fig. 7, the transitions between the normal liquid and the superfluid correspond to the line a-f in Fig. 7, the small two-phase region between tce and qp corresponds to the line

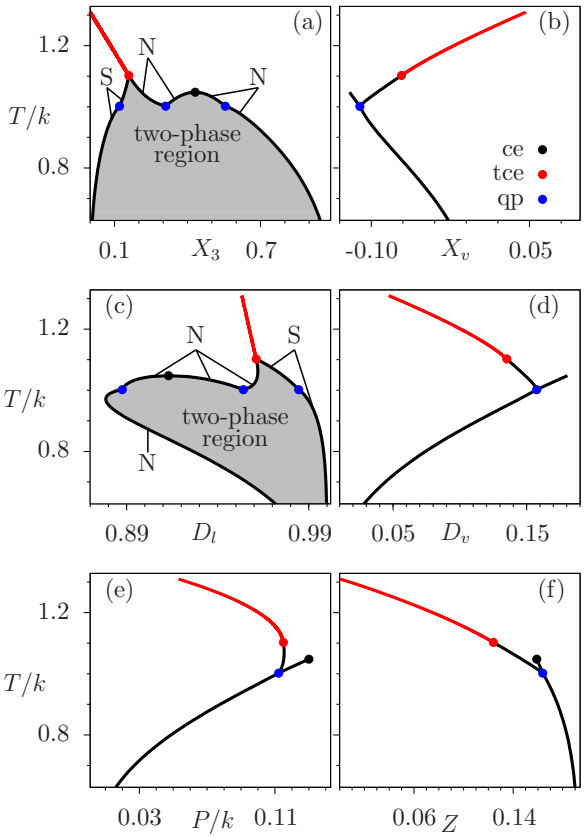

FIG. 11. (Color online) The same as in Fig. 10 but for the coupling constants $(c/k, j/k, j_s/k) = (1, 5.714, 2.747)$ and $H = 0$. At tce the order parameters of the liquid and the vapor phases are $(X_l^{\rm tce}, D_l^{\rm tce}, M_l^{\rm tce}) = (0.644, 0.961, 0)$ and $(X_v^{\rm tce}, D_v^{\rm tce}, M_v^{\rm tce}) = (-0.071, 0.135, 0)$, respectively, and $T_{\rm tce}/k = 1.101$. Again, ce remains as in the case of $j_s = 0$. N and S denote normal liquid and superfluid, respectively. The four coexisting states at the quadruple point qp are given by $(X^{\rm qp}, D^{\rm qp}, M^{\rm qp}) = (-0.222, 0.888, 0), (0.334, 0.954, 0), (0.742, 0.984, 0.456)$, and $(0.110, 0.157, 0)$ at the temperature $T_{\rm qp}/k = 1.001$. The long black lines in (b) and (d) and the ones in (e) and (f) ending at ce are expected to exhibit a break in slope at qp; on the present scales this is not visible.

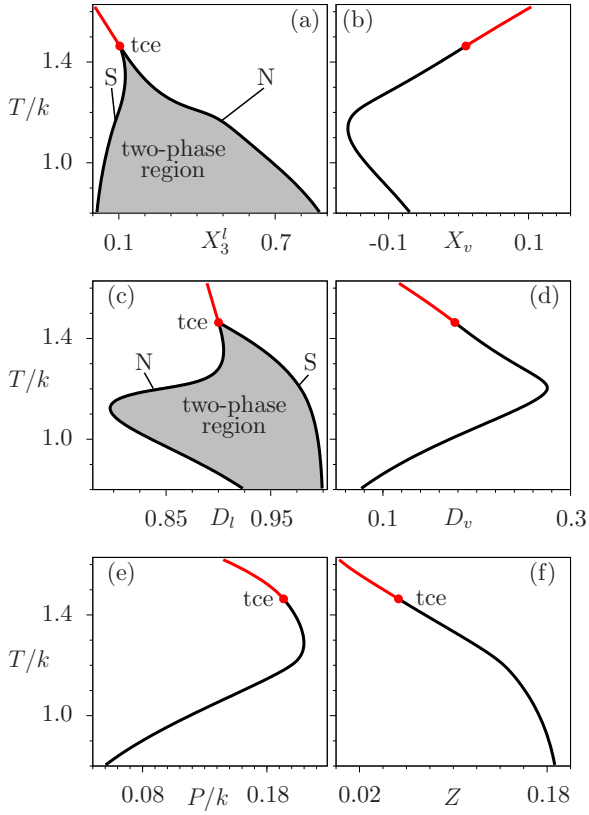

FIG. 12. (Color online) Phase diagrams for the coupling constants $(c/k, j/k, j_s/k) = (1, 5.714, 3.674)$ and $H = 0$, corresponding to Fig. 8. The panels show the same as in Figs. 10 and 11; however, the critical end point ce has disappeared. At tce the liquid state $(X_l^{\rm tce}, D_l^{\rm tce}, M_l^{\rm tce}) = (0.693, 0.900, 0)$ coexists with the vapor state $(X_v^{\rm tce}, D_v^{\rm tce}, M_v^{\rm tce}) = (0.010, 0.176, 0)$ at $T_{\rm tce}/k = 1.462$. For $T > T_{\rm tce}$ there is only a second-order phase transition from a normal mixed liquid to a superfluid. For $T < T_{\rm tce}$ the phase transitions between the normal fluid and the superfluid are first order. N and S denote normal liquids and superfluids, respectively.

f-k in Fig. 7, and the red line above tce corresponds to the red line emanating from k towards h in Fig. 7. In Fig. 7 the triple lines a-f and k-f merge at the quadrupole point qp = f, where four phases coexist: two normal liquids, the superfluid, and the vapor phase. Below qp, the liquid-liquid transitions at coexistence with the vapor phase are first-order transitions between the normal fluid and the superfluid. Upon increasing j_s the tricritical end point tce = k is pulled towards higher temperatures (compare Figs. 10 and 11).

In order to obtain phase diagrams with the topology illustrated in Fig. 8, one has to choose the coupling constants such that the demixing transitions at coexistence with the vapor phase occur only between the normal fluid and the superfluid. This means that in Fig. 7 the line f-c has to shrink to zero, which implies that the critical point c coincides with the quadruple point f. Within Fig. 11(a) this means that tce (=k in Fig. 7) has to be pulled up to higher temperatures such that the demixing critical end point ce (=c in Fig. 7) slides below the quadruple qp (=f in Fig. 7) so the demixing phase transition between two normal fluids becomes an unstable one within the two-phase region of the superfluid and the mixed normal fluid [see Fig. 12(a)]. For the coupling constants $(c/k, j/k) = (1, 5.714)$ this is fulfilled, provided that $j_s/k > 2.96$. For the coupling constants $(c/k, j/k, j_s/k) = (1, 5.714, 2.96)$ at $T_{\rm ce}/k = 1.047$ only three thermodynamic states coexist: the critical state $(X_{\rm ce}, D_{\rm ce}, M_{\rm ce}) = (0.050, 0.913, 0)$, the vapor phase, and a superfluid state $(X_s, D_s, M_s) = (0.756, 0.983, 0.497)$. Accordingly, for coupling constants $(c/k = 1, j/k = 5.714, j_s/k > 2.96)$ one obtains the type of phase diagram shown in Figs. 8 and 12.

As can be inferred from Fig. 12(f), upon increasing the temperature, the line of second-order phase transitions to the superfluid phase (red line) approaches the plane $Z = 0$, where the liquid becomes pure ^{4}He. In order to explore the phase diagram in the plane $Z = 0$, in Eqs. (17) to (21) we have to take the limit $\mu_3 \to -\infty$. In this limit $\Delta_- \to +\infty$ and $\Delta_+ \to -\infty$ so W and R turn into

$$\lim_{\mu_3 \to -\infty} W(\Delta_-, \Delta_+, H, T) = 0, \qquad (42)$$

and, due to $\Delta_- + \Delta_+ = \mu_4$,

$$\lim_{\mu_3\to-\infty} R(\Delta_-,\Delta_+,H,T) = e^{\beta((c+k)X+(j+c)D+\mu_4)}. \quad (43)$$

Since $W_{\mu_3\to-\infty} = 0$, due to Eqs. (17) and (18), one has $X_{\mu_3\to-\infty} = D_{\mu_3\to-\infty}$, where $D_{\mu_3\to-\infty}$ is given by

$$D_{\mu_3\to-\infty} = \lim_{\mu_3\to-\infty} \frac{R(\Delta_-,\Delta_+,H,T)I_0(j_sM/T + H/T)}{1 + R(\Delta_-,\Delta_+,H,T)I_0(j_sM/T + H/T)} = \frac{e^{\beta((j+k+2c)D+\mu_4)}I_0(j_sM/T + H/T)}{1 + e^{\beta((j+k+2c)D+\mu_4)}I_0(j_sM/T + H/T)}, \quad (44)$$

where, due to $X_{\mu_3\to-\infty} = D_{\mu_3\to-\infty}$, in $R_{\mu_3\to-\infty}$ we have replaced X by D.

In this limit Eq. (29) reduces to

$$\frac{D}{M} = \frac{I_0(j_sM/T + H/T)}{I_1(j_sM/T + H/T)} \quad (45)$$

and the equilibrium free energy [Eq. (22)] reduces to

$$\phi(\mu_3 \to -\infty,\mu_4,H,T) = \mathcal{N}\left[\frac{k+j+2c}{2}D^2 + \frac{j_s}{2}M^2 + T\ln(1-D)\right]. \quad (46)$$

In this limit the temperature of the superfluid transition is given by

$$T_s = \frac{j_s}{2}D, \quad (47)$$

and μ_4 follows from Eq. (44):

$$\mu_4(H,T) = T\ln\frac{D}{1-D} - (j+2c+k)D - T\ln I_0(j_sM/T + H/T). \quad (48)$$

For pure ^{4}He, i.e., for $Z = 0$ and for the choice of the coupling constants $(c/k, j/k, j_s/k) = (1,5.714,3.674)$, the phase diagram in the (T, P) plane is shown in Fig. 13. The dashed green line shows the λ-line of second-order phase transitions between normal liquids and superfluids. This line is terminated by the line of first-order liquid-vapor phase transitions (blue line) at the critical end point ce. The line of first-order liquid-vapor phase transitions ends at the critical point c. For high pressures the system becomes solid (see Fig. 1), which, however, is not captured by the present model. Along the line of first-order liquid-vapor transitions ($T > T_{ce}$, blue line in Fig. 13), the difference between the number densities of the liquid and the vapor phases decreases upon increasing the temperature and vanishes at $T = T_c$. Accordingly, the two phases merge into a single phase at the critical point c given by

$$\left.\frac{d\mu_4}{dD}\right|_T = \left.\frac{d^2\mu_4}{dD^2}\right|_T = 0, \quad \left.\frac{d^3\mu_4}{dD^3}\right|_T > 0, \quad (49)$$

where μ_4 is given by Eq. (48). These conditions reduce to [note that $I_0(0) = 1$]

$$D_c = 0.5, \quad T_c = 0.25(2c + j + k). \quad (50)$$

For nonzero values of Z, i.e., in the presence of ^{3}He atoms, the critical points of the phase transitions between vapor and normal liquids ($M = 0$) are given by [see Eqs. (5) and (27)]

$$\left.\frac{d\Delta_+}{dD}\right|_{\Delta_-,T} = \left.\frac{d^2\Delta_+}{dD^2}\right|_{\Delta_-,T} = 0, \quad \left.\frac{d^3\Delta_+}{dD^3}\right|_{\Delta_-,T} > 0, \quad (51)$$

where in Eq. (27) also the partial derivatives of X with respect to D must be taken into account. Having determined various features of the phase diagram of the present model for a set of coupling constants for which the topology of the phase diagram is that of the experimental one, we can illustrate quantitatively the phase diagram in the (P, Z, T) space. The phase diagram, which—for a suitable set of coupling constants—resembles the schematic phase diagram proposed in Ref. [1] and exhibits all relevant fluid phases, is given in Fig. 14 (compare Fig. 3). Accordingly, Fig. 14 shows where the vapor phase (V), the normal liquid phase (N), and the superfluid phase are thermodynamically stable and where first- or second-order phase transitions among each other occur. The transitions between the vapor and the liquid phases are given by the two surfaces o-ce-tce-b-b″-o and ce-c-c′-b-tce-ce (the union of which corresponds to A_2 in Fig. 3), while the loci of the phase transitions between the superfluid and the normal fluid form the two surfaces b-tce-t-b′-b and tce-ce-c″-t-tce which, in Fig. 3, correspond to A_4 and A_3, respectively.

The points o, ce, c, and c″ lie in the zero fugacity plane ($Z = 0$), whereas b′, t, and c″ lie in the plane of constant pressure $P/k = 0.560$. The points b″ and o are located in the plane of constant temperature $T/k = 1.071$, while b, b′, b″, and c′ share the same value of fugacity $Z = 0.139$. The black line b-tce and the light red line tce-ce indicate first- and second-order liquid-liquid phase transitions, respectively, at coexistence with the vapor phase. These two lines are connected at the tricritical end point tce. The dark red solid line (tce-t) connects the surfaces A_4 and A_3 of first- and second-order liquid-liquid phase transitions (b-b′-t-tce-b and t-tce-ce-c″-t), respectively.

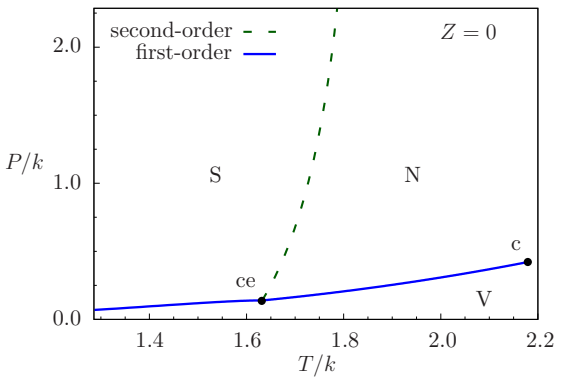

FIG. 13. (Color online) The (T, P) phase diagram for the coupling constants $(c/k, j/k, j_s/k) = (1,5.714,3.674)$ and $H = 0$ for pure ^{4}He, i.e., $Z = 0$. The dashed green line shows the λ-line of second-order phase transitions between normal liquids and superfluids. N, S, and V denote the normal liquid, the superfluid, and the vapor phases, respectively. The blue line of first-order liquid-vapor transitions terminates the λ-line at the critical end point ce and ends at the critical point c of the liquid-vapor coexistence line. (We have been unable to find a set of coupling constants for which the dashed λ-line of second-order phase transitions exhibits a negative slope as it is the case for actual ^{4}He.)

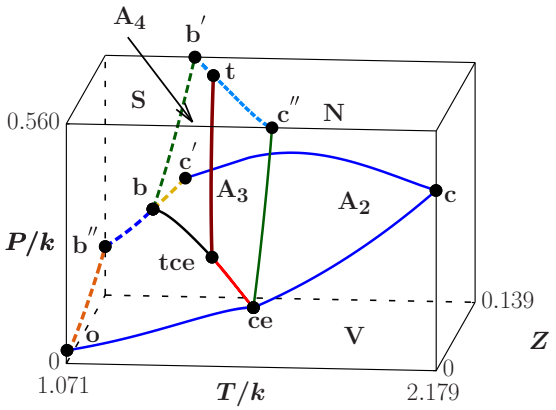

FIG. 14. (Color online) Numerical results for the fluid parts of the phase diagram for the choice of the coupling constants $(c/k, j/k, j_s/k) = (1, 5.714, 3.674)$ and $H = 0$ in (P, Z, T) space. The points o, ce, c, and c″ lie in the zero fugacity plane $(Z = 0)$ and the points c″, t, and b′ lie in the constant pressure plane $P/k = 0.560$. The points o and b″ have the same temperature $T/k = 1.071$, while b, b′, and c′ share the same value of the fugacity $Z = 0.139$. The surface (o-ce-tce-b-b″-o) corresponds to first-order phase transitions between the vapor phase (V) and the superfluid phase (S), whereas (ce-c-c′-b-tce-ce) is the surface of first-order phase transitions between the vapor phase and the normal liquid phase (N); their union corresponds to A_2 in Fig. 3. The surface (b-tce-t-b′-b) is the surface of first-order phase transitions between the superfluid and the normal liquid phase corresponding to A_4 in Fig. 3 and (tce-ce-c″-t-tce) is the surface of second-order phase transitions between the superfluid and the normal liquid phase corresponding to A_3 in Fig. 3. The black line b-tce and the light red line tce-ce are the lines of first- and second-order liquid-liquid transitions at coexistence with the vapor phase, respectively, which meet at the tricritical end point tce. The solid blue line c-c′ is the line of critical points of the liquid-vapor phase transitions and the dark red curve (tce-t) is the line of tricritical points. The lowest pressure is $p/k = 0$, whereas the highest temperature is $T/k = 2.179$. The line o-b″ is the intersection of A_2 and the plane $T/k = 1.071$, the line c′-b-b″ is the intersection of A_2 and the plane $Z = 0.139$; the line b-b′ is the intersection of A_4 with the plane $Z = 0.139$; the line b′-t and t-c″ are the intersection of A_4 and A_3, respectively, with the plane $P/k = 0.560$. We note that at ce the line o-ce-c does not exhibit a break in slope (see Fig. 13).

The coexisting states along the two lines (b-tce, $T < T_{\rm tce}$) and (tce-ce, $T > T_{\rm tce}$) are the ones shown in Fig. 12. The solid blue line (c-c′) is the line of critical points of the liquid-vapor phase transitions and the dark red curve (tce-t) is the line of tricritical points with the tricritical end point tce.

By moving along the line b-b″ towards b″ the number density in the liquid phase increases. This implies that the larger the number density of the liquid phase at b is, the shorter is the line b-b″ (note that $D < 1$). This means that, by lowering the temperature along the line of first-order liquid-liquid phase transitions at coexistence with the vapor phase (tce-b), the point b shifts towards the point b″.

The liquid-liquid phase transitions at constant pressure are given by the curve b′-t-c″. The curve (b′-t) is a line of first-order liquid-liquid phase transitions at constant pressure, which is connected to the line of second-order liquid transitions (t-c″) at the tricritical point t. The coexisting states along these

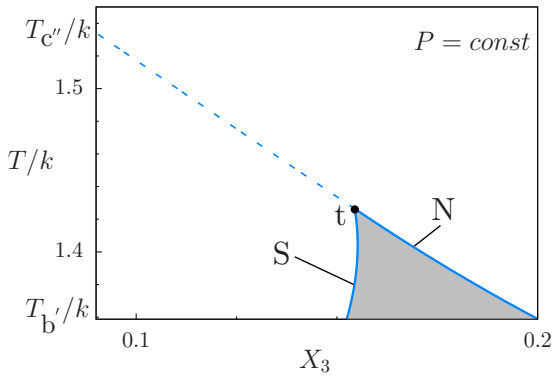

FIG. 15. (Color online) The liquid-liquid phase transitions at fixed pressure $P/k = 0.560$ in the (X_3, T) plane for the choice of the coupling constants $(c/k, j/k, j_s/k) = (1, 5.714, 3.674)$ and $H = 0$. The figure provides the temperature dependence of X_3 along the line b′-t-c″ in Fig. 14. For $T_t < T < T_{c''}$ the light blue dashed line represents continuous phase transitions, whereas for $T_{b'} < T < T_t$ the lines indicate the coexisting superfluid (S) and normal liquid (N) states at first-order phase transitions. The two-phase region is shaded in gray. The point t corresponds to a tricritical point.

two lines are shown in Fig. 15. For even higher pressures the system solidifies, and the two surfaces (A_4, b-tce-t-b′-b) and (A_3, tce-ce-c″-t-tce) should continue towards a surface of first-order liquid-solid phase transitions (see A_1 in Fig. 3) which is not supported by the present model.

V. SUMMARY AND CONCLUSION

The phase diagram of the general vectorized Blume-Emery-Griffiths model has been explored within mean-field theory. The model exhibits a liquid phase, which can be either a superfluid or a normal liquid, and a vapor phase. Depending on the choice of the coupling constants the model exhibits various topologies of the phase diagram. Here we have focused on those topologies of the phase diagram which are associated with liquid-liquid phase transitions at coexistence with the vapor phase. Knowledge of them is a prerequisite for studying tricritical Casimir forces in ^{3}He-^{4}He wetting films. If the coupling constant j_s, which facilitates the occurrence of the superfluid phase, is turned off, the phase diagram is that of a normal binary liquid mixture (see Figs. 4 and 5). For nonzero but small values of this superfluid coupling constant the transitions to the superfluid phase are second order only (Figs. 6 and 9). For larger values of this coupling constant, the transition to the superfluid phase can also be of first order (Figs. 7, 10, and 11); the liquid-liquid phase transitions can be either between two normal liquids or between superfluid and normal liquids. For even larger values of the superfluid coupling constant, the first-order liquid-liquid phase transitions occur only between the superfluid and the normal fluid (Figs. 8 and 12), as it is the case for actual ^{3}He-^{4}He mixtures (see Figs. 1–3).

We conclude that for a suitable set of coupling constants, various features of the phase diagram of ^{3}He-^{4}He mixtures are captured by the present approach (see Figs. 12–15). The detailed knowledge of the bulk phase diagram is necessary

for studying wetting phenomena within the present model and, further, tricritical Casimir forces acting on wetting films. The present model lends itself also for investigations based on Monte Carlo simulations. This model of a binary liquid mixture incorporates vectorial degrees of freedom associated with the ^{4}He particles which covers the more complex behavior of the superfluid order parameter. It is interesting to note that the sequence of the phase diagrams [Figs. 9(a), 10(a), 11(a), and 12(a)] exhibits the identical topologies as the phase diagrams of one-component dipolar fluids upon increasing the dipole strength with the isotropic and ferromagnetic liquid corresponding to the normal liquid and the superfluid, respectively [17,18]. For dipolar fluids the solid phase can be captured by off-lattice density functional theory [19]. Similar topologies have been observed in off-lattice symmetrical binary fluid mixtures [20,21].

[1] M. Krech and S. Dietrich, Phys. Rev. A **46**, 1922 (1992).
[2] M. Blume, V. J. Emery, and R. B. Griffiths, Phys. Rev. A **4**, 1071 (1971).
[3] J. Sivardière and J. Lajzerowicz, Phys. Rev. A **11**, 2090 (1975).
[4] S. Dietrich and A. Latz, Phys. Rev. B **40**, 9204 (1989).
[5] T. Getta and S. Dietrich, Phys. Rev. E **47**, 1856 (1993).
[6] D. Mukamel and M. Blume, Phys. Rev. A **10**, 610 (1974).
[7] J. L. Cardy and D. J. Scalapino, Phys. Rev. B **19**, 1428 (1979).
[8] A. N. Berker and D. R. Nelson, Phys. Rev. B **19**, 2488 (1979).
[9] A. Maciołek, M. Krech, and S. Dietrich, Phys. Rev. E **69**, 036117 (2004).
[10] R. Garcia and M. H. W. Chan, Phys. Rev. Lett. **88**, 086101 (2002).
[11] M. Krech and S. Dietrich, Phys. Rev. A **46**, 1886 (1992).
[12] R. Garcia and M. H. W. Chan, Phys. Rev. Lett. **83**, 1187 (1999).
[13] A. Ganshin, S. Scheidemantel, R. Garcia, and M. H. W. Chan, Phys. Rev. Lett. **97**, 075301 (2006).
[14] A. Maciołek, A. Gambassi, and S. Dietrich, Phys. Rev. E **76**, 031124 (2007).
[15] P. M. Chaikin and T. Lubensky, *Principles of Condensed Matter Physics* (Cambridge University Press, Cambridge, 1995).
[16] M. Abramowitz and I. A. Stegun, eds., *Handbook of Mathematical Functions* (Dover, New York, 1972).
[17] B. Groh and S. Dietrich, Phys. Rev. Lett. **72**, 2422 (1994).
[18] B. Groh and S. Dietrich, Phys. Rev. E **50**, 3814 (1994).
[19] B. Groh and S. Dietrich, Phys. Rev. E **54**, 1687 (1996).
[20] J. Köfniger, N. B. Wilding, and G. Kahl, J. Chem. Phys. **125**, 23450 (2006).
[21] N. B. Wilding, F. Schmid, and P. Nielaba, Phys. Rev. E **58**, 2201 (1998).